# Formation of nanobubbles generated by hydrate decomposition: A molecular dynamics study

Zilin Wang(王梓霖)[1,2], Liang Yang(杨亮)[1,2,†], Changsheng Liu(刘长生)[1,2], and Shiwei Lin(林仕伟)[1,2,‡]

[1] *State Key Laboratory of Marine Resource Utilization in South China Sea, Hainan University, Haikou* 570228, *China*
[2] *School of Materials Science and Engineering, Hainan University, Haikou* 570228, *China*

(Received 7 April 2022; revised manuscript received 14 June 2022; accepted manuscript online 14 June 2022)

Natural gas hydrate is estimated to have huge reserves. Its exploitation can solve the global oil and gas shortage problem. Hydrates decompose into water and methane, and methane molecules are supersaturated to form nanobubbles. Methane nanobubbles can affect the decomposition efficiency of hydrates. They can provide abundant methane sources for the re-nucleation of hydrates. Molecular dynamics is employed in this study to investigate the decomposition process of type I methane hydrate and the formation of methane nanobubbles generated during decomposition under different methane mole fraction, pressures, and temperatures. The results indicate that external pressure inhibits the diffusion of methane molecules, thereby preventing the formation of nanobubbles. A higher mole fraction of methane molecules in the system requires a higher external pressure to generate stable nanobubbles after the decomposition of the hydrate structure. At 330 K, it is easy to form a nanobubble structure. Results of this study can help provide ideas for the study of efficient extraction and secondary nucleation of hydrates.

**Keywords:** molecular dynamics, methane hydrate, nanobubbles, stability

**PACS:** 31.15.xv, 91.50.Hc, 47.55.dd, 36.40.Qv **DOI:** 10.1088/1674-1056/ac786a

## 1. Introduction

Natural gas hydrate (NGH) is composed of water and methane, where water molecules are hydrogen-bonded together to form a cage-like structure.[1] It is an efficient and clean energy source that has enormous reserves around the world.[2] Additionally, the study of gas hydrates has significant environmental implications. For instance, one volume of gas hydrate can release 160 volumes of methane gas.[3,4] Hydrates can serve as gas containers to store methane, reducing the greenhouse effect.[5]

During the decomposition of NGH, methane molecules are released into the liquid water phase, forming methane-rich areas.[6–10] After that, part of the methane molecules form nanobubbles, which overcome the solubility barrier of methane molecules in water.[11] Experiments on NGH decomposition have already proven nanobubbles.[12] The development of computer performance and theoretical research has enabled many scholars to study the NGH decomposition process by molecular dynamics (MD). This method resolves the issue of excessive time and space scales and the lack of structural characterization methods available in experiments.[13–20] Currently, the research on methane nanobubbles focuses primarily on how bubbles affect hydrate decomposition. Nanobubbles will accumulate on the surface of methane hydrate during the decomposition process,[21,22] forming a temperature difference on the surface to slow down the decomposition process. Nevertheless, some researchers have demonstrated that nanobubbles absorb methane molecules during the growth process, reducing the concentration of methane and accelerating hydrate decomposition.[23–26] Additionally, nanobubbles have a high internal pressure that can provide abundant gas sources for hydrate nucleation, significantly impacting secondary hydrate nucleation.[27]

In conclusion, nanobubbles have an essential impact on the efficient utilization of NGH, secondary nucleation of hydrates, and transportation and storage of natural gas. However, it is challenging to study the formation of nanobubbles generated during the decomposition of hydrates due to experimental conditions. The research on the formation of nanobubbles during hydrate dissociation is insufficient. Moreover, external conditions such as methane mole fraction, pressure, and temperature on the formation of nanobubbles generated during hydrate decomposition have not been thoroughly investigated. This paper uses molecular dynamics to examine the effect of external conditions on the decomposition process of type I methane hydrates at the microscopic scale. We will examine the external conditions that can affect the formation of nanobubbles. Moreover, it provides research ideas for the study of hydrate safe exploitation and hydrates secondary nucleation.

[†]Corresponding author. E-mail: yl5923@hainanu.edu.cn
[‡]Corresponding author. E-mail: linsw@hainanu.edu.cn

© 2023 Chinese Physical Society and IOP Publishing Ltd 

## 2. Simulation methods

### 2.1. Building models

As shown in Fig. 1, we construct a methane hydrate–water model to investigate the decomposition and evolution of methane hydrates, with a size of 3.591 nm × 3.591 nm × 14.071 nm. We use a 6 × 6 × 4 supercell[28] of methane hydrate to build the hydrate block. The model contains 161 methane molecules, and water molecules are filled on one side of the hydrate based on the built-in module of LAMMPS. We control the mole fraction of methane molecules in the hydrate by adjusting the amount of water.

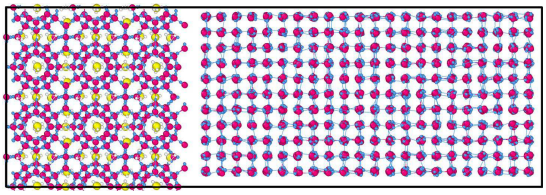


**Fig. 1.** Type I methane hydrate–water initial structural model.

### 2.2. Force fields and simulation details

$CH_4$ and $H_2O$ were modeled using an optimized potentials for liquid simulations united-atom model (OPLS–UA)[29] and SPC[30] force field, respectively. The interaction parameters between atom pairs are shown in Table 1. LAMMPS[31] was used for all simulations. Periodic boundary conditions were applied in three dimensions, and the cutoff distance was set to 1.5 nm. The time step was 1.0 fs. The temperature and pressure were controlled using the Nose–Hoover thermostat with a time constant of 0.1 ps and 1.0 ps, respectively. We used the shake algorithm to maintain the water rigidity.[32]

The main simulation steps include: (i) O atoms and $CH_4$ are fixed from hydrates, and we relax the system in NVT ensemble at 330 K for 100 ps, followed by a 100 ps run in NPT ensemble at 330 K and 0.5 MPa. (ii) Unfix O atoms and $CH_4$. Apply pressures from 0.5 MPa to 40 MPa within the NPT ensemble to study the influence of pressure on the decomposition of NGH and the stability of nanobubble formation; (iii) Under the NPT ensemble, we examine the effect of temperature on the decomposition of NGH and the stability of nanobubble formation at temperatures ranging from 330 K to 360 K.

**Table 1.** Atom pair interaction parameters.

| Atom pairs | $\sigma$ (Å) | $\varepsilon$ (eV) |
|---|---|---|
| Cm–Hm | 4.0000 | 0.0020810 |
| Cm–Cm | 3.5000 | 0.0028620 |
| Hw–Hw | 0.0000 | 0.0000000 |
| Hw–Hm | 1.5000 | 0.0013010 |
| Hw–Cm | 2.2000 | 0.0019300 |
| Hm–Hm | 4.5000 | 0.0013000 |
| Ow–Ow | 3.1656 | 0.0067366 |
| Ow–Hw | 0.0000 | 0.0000000 |
| Ow–Cm | 3.6270 | 0.0052910 |
| Ow–Hm | 2.7770 | 0.0035150 |

As part of the calculation, the spatial conformation of water is examined with $F_3$ and $F_4$ order parameters, and the rate of hydrate structure decomposition is indirectly examined. We apply the mean shift algorithm[33] to detect methane nanobubbles generated during the decomposition of NGH. The mean shift algorithm originally represents a shifted mean vector and now refers to an iterative step. The specific process is first to find the offset mean of the current point and then use it as a new starting point to continue moving until the end condition is met. The mean shift algorithm is currently used in various fields, including clustering applications, image smoothing, and object tracking. We use the root mean square displacement (RMSD) to characterize the movement of methane molecules during hydrate decomposition, which can be defined as

$$\mathrm{RMSD} = \sqrt{\sum_{i=1}^{N} \left\langle |r(t) - r(0)|^2 \right\rangle}, \tag{1}$$

where $r(0)$ and $r(t)$ are the initial and final positions of the atom, respectively.

### 2.3. Order parameter

Previous research has commonly utilized the three-body order parameter $F_3$ and the four-body order parameter $F_4$ to characterize hydrate structures.[34,35] The $F_3$ parameter refers to three water molecule configurations that describe the degree of deviation of a tetrahedron formed by a central oxygen atom and other oxygen atoms from the regular tetrahedron, which can be defined as

$$\begin{aligned} F_3 &= \frac{1}{n_i(n_i-1)/2} \\ &\quad \times \sum_{j=1}^{n_i-1} \sum_{k=j+1}^{n_i} \left( \left|\cos\theta_{jik}\right| \cos\theta_{jik} + \cos^2(109.47^\circ) \right)^2 \\ &= \frac{1}{n_i(n_i-1)/2} j \\ &= 1ni - 1k \\ &= j + 1ni \left( \left|\cos\theta_{jik}\right| \cos\theta_{jik} + \frac{1}{9} \right)^2, \end{aligned} \tag{2}$$

where $n_i$ represents the nearest neighbours of water molecule $i$. $\theta_{jik}$ provides the angle between the oxygen atoms in water molecules $j$, $i$, and $k$. The $F_3$ value of solid water and hydrate is 0.01, while the $F_3$ value of liquid water is 0.1.

The order parameter $F_4$ is the dihedral angle formed by the outermost hydrogen and oxygen of two adjacent water molecules, which can be defined as

$$F_4 = \frac{1}{n} \sum_{i=1}^{n} \cos 3\phi_i, \tag{3}$$

where $n$ is the number of water–water pairs. $\phi_i$ is the O–H torsion angle of two adjacent water molecules. The $F_4$ values for some systems are as follows: −0.4 for ice, −0.04 for liquid water, and 0.7 for hydrate (type I hydrate: 0.89; type II hydrate: 0.96).

## 3. Results and discussion

### 3.1. Hydrate decomposition process

As hydrate decomposes, its potential energy increases gradually because of its endothermic nature. Thus, the potential energy change of the system can be related to the rate of hydrate decomposition. Figure 2(a) illustrates the variation trend of potential energy as a function of the temperature during the decomposition of NGH with a methane mole fraction of 0.046. As the temperature increases from 330 K to 360 K, it can be seen that the increase rate of the potential energy curve continues to rise, and it also plateaus more rapidly. This trend means that the hydrate structure decomposes more rapidly with increased temperature, which indicates that the hydrate decomposition process is more sensitive to temperature than methane mole fraction or external pressure (Fig. S1 in supplementary information).

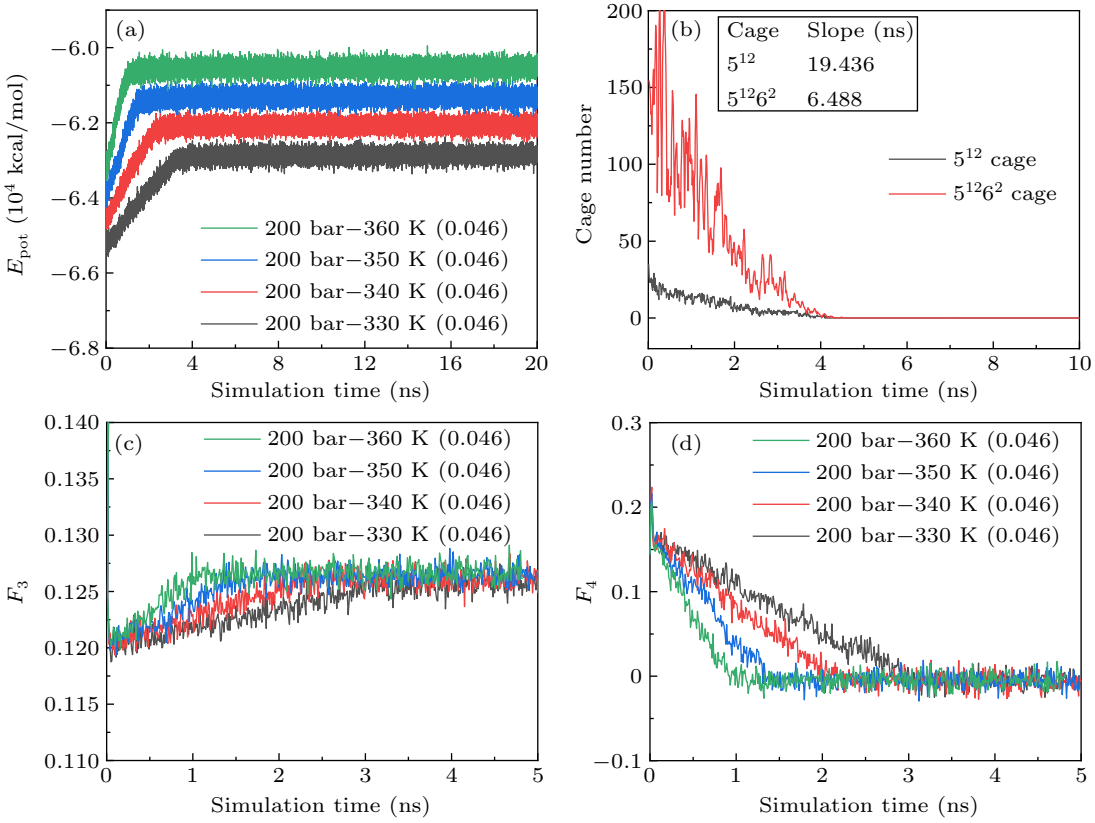



**Fig. 2.** (a) Potential energy during hydrate dissociation at 330 K–360 K. (b) The number of $5^{12}$ and $5^{12}6^2$ cages during hydrate decomposition at 330 K. (c) $F_3$ order parameter during hydrate dissociation at 330 K–360 K. (d) $F_4$ order parameter during hydrate dissociation at 330 K–360 K.

A type I hydrate can contain six large cages ($5^{12}6^2$) and two small cages ($5^{12}$). Figure 2(b) illustrates the variation in cage types during the decomposition process. Accordingly, the decomposition rates of cages $5^{12}$ and $5^{12}6^2$ are 6.488 $ns^{-1}$ and 19.436 $ns^{-1}$, respectively, and cage $5^{12}6^2$ decomposes at a rate approximately three times than that of cage $5^{12}$.[36] It corresponds to the ratio of cage sizes in the hydrate crystal structure, demonstrating that gas hydrates do not decompose locally but within the individual cells.

Figures 2(c) and 2(d) show the order parameters $F_3$ and $F_4$ as a function of temperature during the hydrate decomposition. The hydrate structure decomposes completely when the $F_3$ approaches 0.125 and the $F_4$ approaches 0. At 330 K, the hydrate structure is decomposed completely in approximately 3.5 ns. As the temperature rises, the hydrate decomposition rate increases. At 360 K, the hydrate decomposition rate reaches a maximum value, and the structure is wholly decomposed within 1 ns. These results indicate that the hydrate decomposition rate increases with increasing temperature.

Additionally, we studied the changes in order parameters resulting from the hydrate decomposition under various methane mole fractions and external pressures (Fig. S2 in supplementary information). We found that the methane mole fraction and pressure have little effect on the rate of hydrate decomposition.

### 3.2. The formation of methane nanobubbles

#### 3.2.1. Evolution of nanobubbles

As shown in Fig. 3, the microscopic development of methane nanobubbles is illustrated by several typical structures as the hydrate–water system evolves.

Figure 3(a) shows the initial structure. Figure 3(b) de-

picts the optimized model. The density of water molecules has reached an average level (the density is approximately 1 g/cm$^3$), and the hydrate structure is still intact. As the hydrate structure decomposes, methane molecules escape from the cage structure and enter the water phase. At the interface between hydrate and water, methane forms small clusters due to the high local density of methane. Small methane clusters are not stable and often disintegrate and disappear, as shown in Fig. 3(c). Methane clusters may also form methane nanobubbles by absorbing methane molecules in the solution, as shown in Fig. 3(d). When a nanobubble structure is unstable, it usually decomposes and disappears (Fig. 3(c)) or transforms into a cylindrical nanobubble structure (Fig. 3(e)) or a methane gas layer structure (Fig. 3(f)).

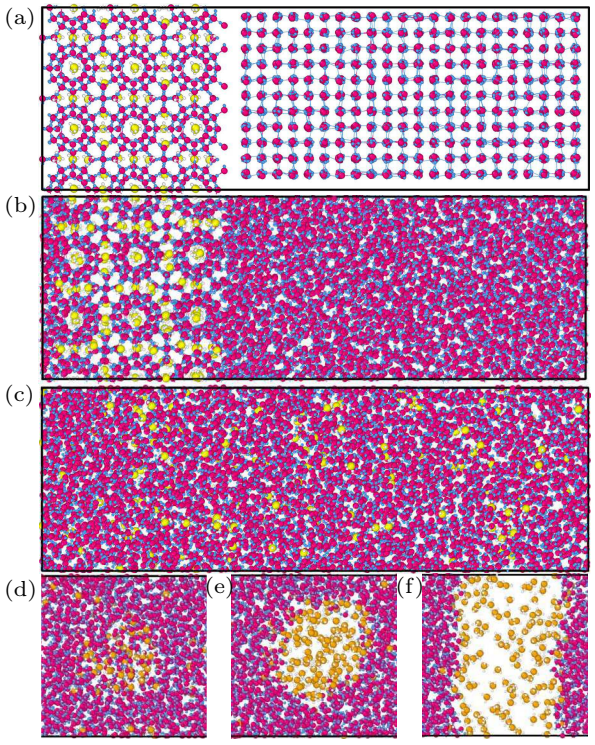



**Fig. 3.** Typical structural evolution process diagram during the molecular dynamics simulation: (a) initial model structure of the methane hydrate–water; (b) optimized structure when hydrate structure is intact; (c) the hydrate structure is completely decomposed; (d) methane molecules form nanobubbles structure; (e) methane molecules form cylindrical nanobubble structure; (f) methane molecules form gas layer structure. The red, blue, yellow, and white balls represent O, H ($H_2O$), C, and H ($CH_4$) atoms, respectively.

### 3.2.2. The effect of $CH_4$ mole fraction on the formation of nanobubbles

We use the mean shift algorithm to analyze the formation of nanobubbles during the hydrate decomposition. The abscissa represents the simulation time, which should be kept longer than 100 ns, and the ordinate represents the number of methane molecules present in the nanobubble. An average number of molecules in a methane cluster exceeding 80 molecules is considered as a criterion for forming nanobubble structures. Specifically, the large vibration amplitude of the curve, as shown in the curve of 10 ns–40 ns in Fig. 4, will result in a cylindrical nanobubble. The gas layer structure often appears after the cylindrical bubble structure, and the number of molecules is usually less than 40. It is worth noting that the cylindrical bubble structures and gas layer structures formed here result from the finite-size effects. When the system increases, these bubble structures will become spherical bubbles to reduce the surface tension.

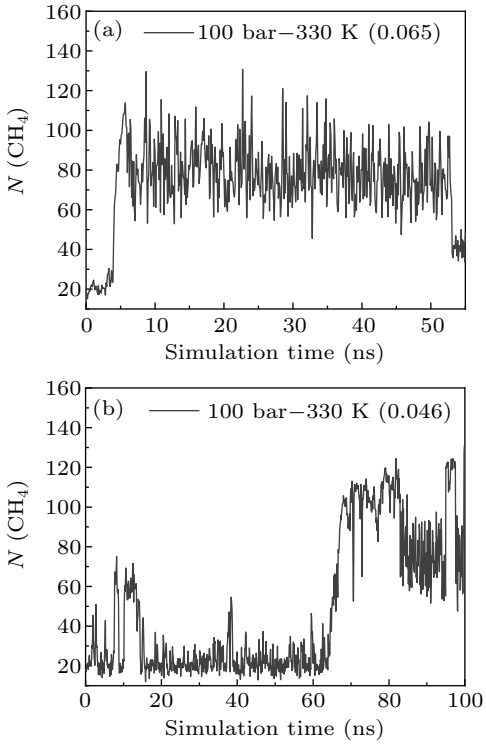



**Fig. 4.** Formation of nanobubbles during the decomposition of methane hydrate. (a) The methane mole fraction for the model is 0.065. (b) The methane mole fraction for the model is 0.046.

As shown in Fig. 4, we investigate the effect of methane mole fraction on the stability of nanobubbles during hydrate decomposition. Figure 4(a) presents the structure with a methane mole fraction of 0.065. At around 7 ns, methane forms nanobubbles that contain about 100 molecules, and its shape is shown in Fig. 3(d). As a result of the high methane concentration in the aqueous solution, the initially formed nanobubbles will gradually grow. At the beginning of the growth process, the nanobubbles will grow radially in all directions. However, due to periodic boundary conditions, the tiny methane bubbles will expand and form cylindrical bubbles to reduce surface tension at about 10 ns. These cylindrical bubbles contain about 80 methane molecules. As simulation time increases, the cylindrical nanobubbles absorb the methane molecules in the aqueous solution. They steadily form a methane gas layer at 52 ns, as illustrated in Fig. 3(f).

As the simulation time increases, the methane molecules in the liquid phase continue to enter the gas layer structure. In the end, the methane molecules in the aqueous solution have almost disappeared. Figure 4(b) presents the structure with a methane mole fraction of 0.046. Due to the decreasing mole fraction of methane, no methane gas layer is formed throughout the simulation time. Methane forms a nanobubble structure around 68 ns, but it is not stable. It will transform into a cylinder bubble structure at around 85 ns.

It is worth noting that the size and shape of methane nanobubbles formed during methane hydrate decomposition may be affected by the size of the simulated box. If a larger simulation box is used, the methane molecules released in the liquid phase may not coalesce to form cylindrical nanobubble. Therefore, the nanobubbles may remain spherical, and the maximum diameter may be influenced by the size of the simulation box. Simulations that study the dependence of bubble size on the simulation box can quantify this dependence. Some theoretical computational work[37] has investigated how the size of the simulation box determines the effective nanobubble concentration in the liquid phase and how it affects the size of the nanobubbles observed in the simulations.

To characterize the distribution of methane molecules during the hydrate decomposition, we calculate the radial distribution function of the C–C atoms (Fig. S6 in supplementary information). Figure S6(a) shows the radial distribution function of hydrate structure. The first peak is at 0.660 nm, which represents the average of the closest distances between methane molecules in the hydrate cage. As time increases, the peak at 0.660 nm gradually decreases, representing the decomposition of the hydrate. At the same time, a new peak appears at 0.400 nm, which means that the methane molecules escape from the cage and form nanobubbles.

The root mean square displacement (RMSD) measures the degree of atom movement relative to their initial position. To understand the movements of methane molecules during the hydrate decomposition, we evaluate the RMSD of carbon atoms.

Figure 5 depicts the RMSD of carbon atoms as a function of methane mole fraction. As the methane mole fraction increases, the amplitude of motion for methane molecules increases. According to Table 2, the diffusion coefficient of methane molecules can be determined by fitting a linear model to the RMSD image. It is worth noting that the diffusion coefficient here refers to the diffusion coefficient of carbon atoms in the whole system. As shown in Table 3, the diffusion coefficient of methane molecules in an aqueous solution is much smaller than that of methane in nanobubbles. Therefore, when the methane bubble structure is formed, the diffusion rate of carbon atoms in the system can be used to approximate the diffusion rate of carbon atoms in methane nanobubbles.

**Table 2.** Diffusion coefficient table.

| System (mole fraction) | Hydrate decomposition ($nm{\cdot}ns^{-1}$) | Methane nucleation (non-nucleation) ($nm{\cdot}ns^{-1}$) | A stable state ($nm{\cdot}ns^{-1}$) |
|---|---|---|---|
| 0.065 | 0.244 | 0.116 | 0.511 |
| 0.052 | 0.321 | 0.139 | 0.059 |
| 0.046 | 0.330 | 0.075 | 0.119 |

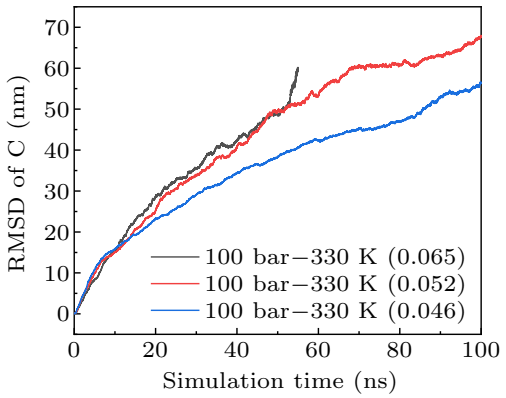



**Fig. 5.** RMSD of carbon atoms at different mole fraction of methane molecules.

There are few differences in methane diffusion rates during hydrate decomposition for structures with different methane mole fractions. The methane diffusion rate increases rapidly at around 52 ns for the system with a methane mole fraction of 0.065. This is due to the formation of a methane gas layer structure. When the hydrate decomposes completely, the methane diffusion rates decrease as the methane mole fraction increases. It is because the higher the concentration of methane molecules, the easier it is to nucleate during the decomposition of hydrates, which then hinders methane diffusion.

As explained above, when the mole fraction of methane is above 0.065, we find that methane molecules are easily nucleated, but the nanobubble structure is not stable. Nanobubble will eventually transform into a gas layer structure. When the mole fraction of methane in the system decreases, the gas layer structure will be replaced by the cylindrical and sphere bubble structures. However, when the mole fraction of methane is lower than 0.044, nanobubbles will not form. The system is more likely to develop stable sphere methane bubble structures with a methane mole fraction of 0.046.

### 3.2.3. The effect of pressure on the formation of nanobubbles

Figure 6 illustrates the effect of pressure conditions on the stability of nanobubbles with a methane mole fraction of 0.046.

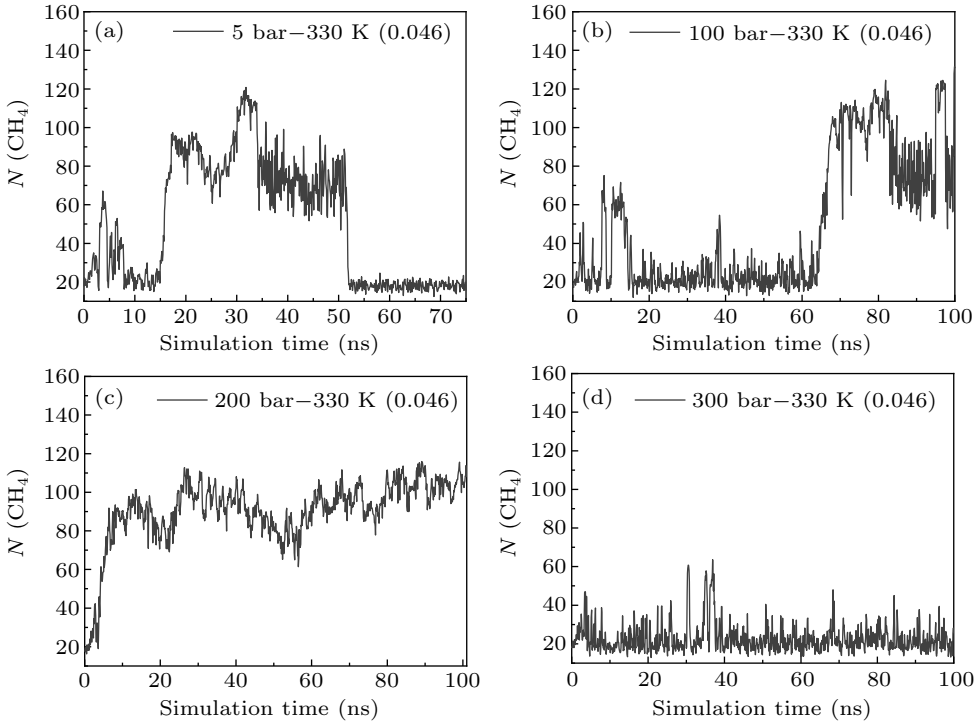



**Fig. 6.** Formation of nanobubbles during the decomposition of methane hydrate. (a) 5 bar; (b) 100 bar; (c) 200 bar; (d) 300 bar.

In Fig. 6(a), methane forms a cylindrical bubble at around 35 ns. At 50 ns, cylindrical nanobubbles absorb methane from the solution and eventually form a layer of methane gas. Figure 6(c) shows that the entire decomposition process creates a stable nanobubble at 200 bar. As shown in Fig. 6(d), once the pressure reaches 300 bar, the simulation will not generate any methane bubbles. This phenomenon can be explained by the Henry's law. In physical chemistry, the Henry's law states that the amount of dissolved gas in a liquid is proportional to its partial pressure above the liquid, which can be defined as

$$C = kP_{\text{gas}}, \tag{4}$$

where $C$ represents the solubility of a gas at a fixed temperature in a particular solvent; $k$ is the Henry's law constant, $P_{\text{gas}}$ is the partial pressure of the gas. Therefore, when the external pressure reaches 300 bar, methane molecules can be dissolved in the aqueous solution, and the methane cluster structure will not be generated. At the same time, we calculate the formation of nanobubbles for model structures with a methane mole fraction of 0.065 (Fig. S3 in supplementary information).

Figure 7 depicts the RMSD of carbon atoms as a function of pressure. As the hydrate dissociates, the movement amplitude of methane is similar at different pressures. This result indicates that the hydrate dissociation rate is virtually the same at various pressures. As shown in Table 3, the methane diffusion rate gradually decreases with the increasing pressure when the hydrate structure has wholly decomposed. Additionally, we calculate the RMSD of carbon atoms in a system with a methane mole fraction of 0.065 (Fig. S4(a) and Table S1 in supplementary information). Hence, the increased pressure may hinder the diffusion of methane molecules.

**Table 3.** Diffusion coefficient table.

| System (pressure) | Hydrate decomposition ($\text{nm}\cdot\text{ns}^{-1}$) | Methane nucleation (non-nucleation) ($\text{nm}\cdot\text{ns}^{-1}$) | A stable state ($\text{nm}\cdot\text{ns}^{-1}$) |
|---|---|---|---|
| 5 bar | 0.389 | 0.108 | 0.965 |
| 100 bar | 0.330 | 0.075 | 0.119 |
| 200 bar | 0.280 | 0.057 | 0.032 |
| 400 bar | 0.277 | 0.072 | 0.072 |

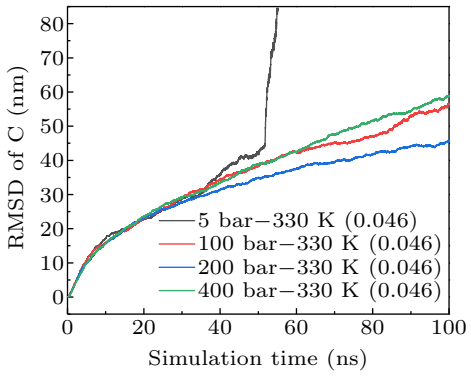



**Fig. 7.** RMSD of carbon atoms at different pressure of methane molecules.

In hydrate decomposition, relatively high pressures can inhibit the diffusion of methane molecules, thereby inhibiting the formation of nanobubbles. It is more feasible to form nanobubbles under low pressure. However, when the external pressure is too low, the methane molecules in the sys-

tem will eventually create a gas layer. For the structures with methane mole fraction of 0.046, 0.052, and 0.065, stable sphere nanobubbles will form when the external pressure is about 200 bar, 300 bar, and 1000 bar, respectively. Because of this, during the NGH decomposition, high external pressure is required to generate stable nanobubbles in an increased methane concentration structure.

### 3.2.4. The effect of temperature on the formation of nanobubbles

As shown in Fig. 8, we use a structure with a 0.046 mole fraction to determine the effect of temperature conditions on the stability of nanobubbles.

Figure 8(a) illustrates the stability of nanobubbles at 5 bar. A methane gas layer structure appears during hydrate decomposition with low pressure. The formation time of the gas layer increases with increasing temperature. As shown in Fig. 8(b), the cylindrical bubble gradually replaces the spherical bubble structure as the temperature increases from 330 K to 350 K at 100 bar. When the temperature reaches 360 K, methane molecules form a gas layer structure around 102 ns. As shown in Fig. 8(c), a stable nanobubble can persist for a long time at 330 K. However, the nanobubble's stability decreases as the temperature rises. The simulation does not generate any nanobubbles at 350 K. In addition, we calculate the formation of nanobubbles for model structure with a methane mole fraction of 0.052 (Fig. S5 in supplementary information).

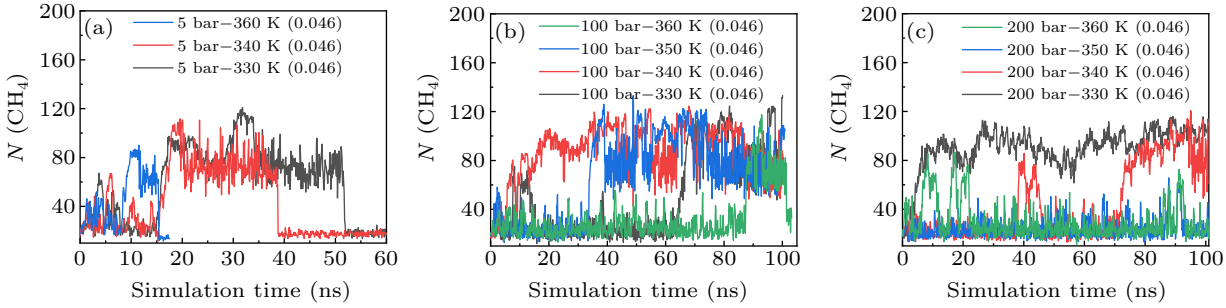



**Fig. 8.** The effect of temperature on the stability of nanobubbles at (a) 5 bar; (b) 100 bar; (c) 200 bar.

Figure 9 depicts the variation of methane movement amplitude with temperature during hydrate decomposition. We find that the initial stages of methane movement at different temperatures are very similar. As simulation time increases, the magnitude of the methane movement will suddenly change at a particular time. As the temperature increases, the time for the sudden transformation gradually advances.

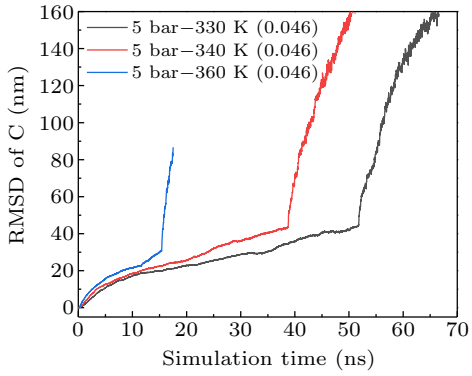



**Fig. 9.** RMSD of carbon atoms at different temperature of methane molecules.

We can fit a linear model to the RMSD image to get the diffusion coefficient of methane molecules. Table 4 displays the diffusion rates of methane molecules under different temperature conditions. In addition, we investigate the diffusion rate of methane molecules under conditions of varying methane mole fraction and other external pressures (Fig. S4 and Tables S2 and S3 in supplementary information). We find that the diffusion rate of methane molecules increases gradually with increasing temperature at each stage. In comparing the diffusion rates of methane molecules at 330 K and 360 K, the diffusion rate increases from 0.389 nm·ns$^{-1}$ to 0.747 nm·ns$^{-1}$ during hydrate decomposition, and it increases by about 1.9 times.

**Table 4.** Diffusion coefficient table.

| System (temperature) | Hydrate decomposition (nm·ns$^{-1}$) | Methane nucleation (non-nucleation) (nm·ns$^{-1}$) | A stable state (nm·ns$^{-1}$) |
|---|---|---|---|
| 330 K | 0.389 | 0.108 | 0.965 |
| 340 K | 0.576 | 0.151 | 1.476 |
| 360 K | 0.747 | 0.231 | 3.734 |

In conclusion, although the decomposition rate of methane hydrate is relatively slow at the lower temperature of 330 K, the existence of nanobubbles in the process is somewhat more stable. When the temperature increases, the methane diffusion rate in the system increases, leading to the instability of methane nanobubbles. As a result, the partially spherical bubbles will gradually transform into cylindrical structures. When the temperature rises to 360 K, the system forms a methane gas layer structure under relatively

low pressure. However, the system will not produce a stable nanobubble structure if the pressure is relatively high because of pressure-induced inhibition of methane diffusion. The simulation results indicate that it is optimal for forming stable sphere nanobubble structures at 330 K.

## 4. Conclusion and perspectives

We find methane mole fraction and external pressure have little effect on hydrate decomposition rate. On the contrary, hydrate structure is more sensitive to temperature change. According to the research on the formation of nanobubbles, methane nanobubbles will not be generated after the hydrate decomposition when the mole fraction of methane is lower than 0.046. When the methane mole fraction is greater than 0.046, the system will likely form stable nanobubble structure. With molecular methane mole fraction of 0.046, 0.052, and 0.065, relatively stable methane nanobubbles are created at 200 bar, 300 bar, and 1000 bar, respectively. As temperatures increase, the diffusion rate of methane molecules in the system increases, making the nanobubbles unstable. It is optimal for forming relatively stable nanobubble structures at 330 K.

## Acknowledgments

The author would like to thank Dr. Liang Yang at Hainan University for useful guidance and discussion during the molecular dynamics study. Project supported by the specific research fund of the Innovation Platform for Academicians of Hainan Province of China and the Hainan Provincial Natural Science Foundation of China (Grant No. 519MS025).

## References

[1] Sloan Jr E D and Koh C A 2007 *Clathrate Hydrates of Natural Gases* (Boca Raton: CRC Press) pp. 45–50
[2] Makogon Y F 2010 *J. Nat. Gas Sci. Eng.* **2** 49
[3] Boswell R, Rose K, Collett T S, Lee M, Winters W, Lewis K A and Agena W 2011 *Mar. Petrol. Geol.* **28** 589
[4] Chong Z R, Yang S H B, Babu P, Linga P and Li X S 2016 *Appl. Energ.* **162** 1633
[5] Cabrera-Ramírez A, Arismendi-Arrieta D J, Valdés A and Prosmiti R 2020 *ChemPhysChem* **22** 359
[6] Bagherzadeh S A, Englezos P, Alavi S and Ripmeester J A 2012 *J. Chem. Thermodyn.* **44** 13
[7] Forrisdahl O K 1996 *Mol. Phys.* **89** 819
[8] John S T and Klug D D 2002 *Supramol. Chem.* **2** 467
[9] Uddin M and Coombe D 2014 *J. Phys. Chem. A* **118** 1971
[10] Vatamanu J and Kusalik P 2007 *J. Chem. Phys.* **126** 124703
[11] Uchida T, Yamazaki K and Gohara K 2016 *Korean J. Chem. Eng.* **33** 1749
[12] Katsuki D, Ohmura R, Ebinuma T and Narita H 2008 *J. Appl. Phys.* **104** 083514
[13] Hawtin R W, Quigley D and Rodger P M 2008 *Phys. Chem. Chem. Phys.* **10** 4853
[14] Jacobson L C, Hujo W and Molinero V 2010 *J. Am. Chem. Soc.* **132** 11806
[15] Jacobson L C and Molinero V 2011 *J. Am. Chem. Soc.* **133** 6458
[16] Liang S and Kusalik P G 2011 *Chem. Sci.* **2** 1286
[17] Moon C, Taylor P C and Rodger P M 2003 *J. Am. Chem. Soc.* **125** 4706
[18] Vatamanu J and Kusalik P G 2010 *Phys. Chem. Chem. Phys.* **12** 15065
[19] Walsh M R, Beckham G T, Koh C A, Sloan E D, Wu D T and Sum A K 2011 *J. Phys. Chem. C* **115** 21241
[20] Walsh M R, Hancock S H, Wilson S J, Patil S L, Moridis G J, Boswell R, Collett T S, Koh C A and Sloan E D 2009 *Energ. Econ.* **31** 815
[21] Kim H, Bishnoi P R, Heidemann R A and Rizvi S S 1987 *Chem. Eng. Sci.* **42** 1645
[22] Ripmeester J A, Alireza S, Hosseini B, Englezos P and Alavi S 2010 *Canadian Unconventional Resources and International Petroleum Conference*, October 19–21, 2010, Alberta, Canada, p. 138112
[23] Fang B, Ning F, Ou W, Wang D, Zhang Z, Yu Y, Lu H, Wu J and Vlugt T J 2019 *Fuel* **258** 116106
[24] Gao F, Gupta K M, Yuan S and Jiang J 2018 *Mol. Simulat.* **44** 1220
[25] Ji H, Chen D, Zhao C and Wu G 2018 *J. Phys. Chem. C* **122** 1318
[26] Yagasaki T, Matsumoto M, Andoh Y, Okazaki S and Tanaka H 2014 *J. Phys. Chem. B* **118** 1900
[27] Chen C, Hu W, Yang L, Zhao J and Song Y 2021 *J. Mol. Liq.* **323** 114614
[28] McMullan R K and Jeffrey G 1965 *J. Chem. Phys.* **42** 2725
[29] Jorgensen W L and Tirado-Rives J 1988 *J. Am. Chem. Soc.* **110** 1657
[30] Berendsen H J, Postma J v, van Gunsteren W F, DiNola A and Haak J R 1984 *J. Chem. Phys.* **81** 3684
[31] Plimpton S 1995 *J. Comput. Phys.* **117** 1
[32] Ryckaert J P, Ciccotti G and Berendsen H J 1977 *J. Comput. Phys.* **23** 327
[33] Fukunaga K and Hostetler L 1975 *IEEE Trans. Inform. Theory* **21** 32
[34] Bagherzadeh S A, Alavi S, Ripmeester J and Englezos P 2015 *J. Chem. Phys.* **142** 214701
[35] Walsh M R, Koh C A, Sloan E D, Sum A K and Wu D T 2009 *Science* **326** 1095
[36] Sloan E D 2003 *Nature* **426** 353
[37] Weijs J H, Seddon J R T and Lohse D 2012 *ChemPhysChem* **13** 2197